*Solid State Science and Technology, Vol. 29, No 1 & 2 (2021) 47-56*
ISSN 0128-7389 | *http://myjms.mohe.gov.my/index.php/masshp*

# SUPERCONDUCTING PROPERTIES OF $Eu_2O_3$ NANOPARTICLES SUBSTITUTION IN Bi(Pb)-2223 CERAMICS

Nurbaisyatul Ermiza Suhaimi[1], Azhan Hashim[2*],
Siti Fatimah Saipuddin[1,2] and Wan Aizuddin Wan Razali[2]

[1]*Faculty of Applied Sciences, Universiti Teknologi MARA Shah Alam, 40450 Shah Alam, Selangor, Malaysia*

[2]*Faculty of Applied Sciences, Universiti Teknologi MARA Pahang, 26400 Bandar Tun Abdul Razak Jengka, Pahang, Malaysia*

**Corresponding author: dazhan@uitm.edu.my*

*Received: 2 December 2021*
*Accepted: 23 December 2021*

## ABSTRACT

This research reports on the effect of $Eu_2O_3$ nanoparticles on structural and superconducting properties of Bi(Pb)-2223 superconductor. Samples were produced through solid state reaction method. The prepared samples have been analyzed through critical temperature ($T_c$), critical current density ($J_c$), X-ray diffraction (XRD), Field Emission Scanning Electron Microscopy (FESEM) and Alternating Current Susceptibility (ACS). Both Bi-2212 and Bi-2223 phases have been detected for all prepared samples with different ratios. The microstructure for all samples shows randomly distributed plate-like grains. The crystallite size was estimated from XRD while the critical temperature ($T_c$) has been determined from resistivity measurements in the range of 30 – 300 K. The maximum calculated $J_c$ was obtained at the sample with $x$ = 0.0025 $Eu_2O_3$ nanoparticles substitution. The best amount of doping was found at $x$ = 0.0025 which improved the superconducting properties of this system.

*Keywords: Bi(Pb)-2223; Rare earth nanoparticles; $Eu_2O_3$ doping; AC susceptibility; Crystallite size*

## INTRODUCTION

In the past decade, numerous applications in technology and industry have been investigated using Bi-based ceramic materials. Superconductors have undergone extensive research and achieved substantial improvement in their superconducting properties and fabrication processes, making them especially well-suited for high-field magnets and electric power systems. In the family of high temperature superconductors, the Bi-based is one of the most promising systems due to its outstanding performance in the electronic areas, high critical temperature ($T_c$), high critical current densities ($J_c$), high magnetic field carrying capacity and their distinctive layered crystal structure [1]. The general composition of the Bi-based (BSCCO) system can be defined as $Bi_2Sr_2Ca_{n-}$

$_1Cu_nO_{2n+4+y}$ where n = 1, 2 and 3 indicates the number of $CuO_2$ layers in the crystal structure. Three different phases of Bi-based materials exhibit the superconductivity at the different critical transition temperature, $T_c$ where Bi-2201 (~ 20 K), Bi-2212 (~ 80-95 K) and Bi-2223 (~110 K) [2,3]. Although Bi-2223 phase appears to be the most promising phase because of its highest superconducting transition temperature, it is considered as a difficult task to produce the series and requires a very long processing time [4].

The effect of doping rare earth oxides and some other oxides on the superconducting and structural properties of BSCCO systems has been studied by a number of researchers. In spite of this, small addition or doping elements in their chemical composition with different ionic radii might affect their superconducting properties, which is why Mohamed et al. [5] pointed out that the dopant characteristics can either enhance or destroy superconducting properties based on their chemical composition. In BSCCO systems, Lead (Pb) plays the most important role in microstructure, phase composition, and superconducting behaviors. The initial mixture containing Pb might favor the formation of the Bi(Pb)-2223 phase. It is nearly impossible to prepare the Bi(Pb)-2223 phase as a single phase since it usually intermixes with the Bi(Pb)-2212 phase.

In order to boost the connectivity between the grains in the Bi(Pb)-2223 superconductor system, it is of interest to incorporate nano-sized rare earth elements. Thus, the objective of this research is to identify the optimum concentrations for Bi(Pb)-2223 superconductor which is prepared using conventional solid state method, as well as to investigate the influence of substituting Eu nanoparticles for Ca site on the structural and electrical properties of Bi(Pb)-2223.

## METHODOLOGY

In this research, solid state reaction method was used to prepare the samples with chemical composition of $Bi_{1.6}Pb_{0.4}Sr_2Ca_{2-x}Eu_xCu_3O_y$ ($x$ = 0.0000, 0.0025, 0.0200, 0.0500, and 0.1000). The powders were mixed with an absolute ethanol for 24 hours using milling machine. The resultant grey slurry was dried for six hours at 120$^o$C in an oven. Upon drying, the grey powder was scraped from the beaker and ground in a mortar for 30 minutes. Two calcination process was performed for 15 hours at 800$^o$C and 830$^o$C respectively with intermediate grinding for one hour in between. Pellets were then created by pressing 2 g of powders for each sample under a pressure of 30 MPa. The furnace's temperature was raised up to 850$^o$C at a rate of 3°C per minute and the pellets was kept for 48 hours for sintering process.

XRD measurement was carried out using X'Pert PRO PANalytical X-ray Diffractometer in the range $2\theta = 5° – 90°$ at room temperature. Microstructural analyses were taken using Field Emission Scanning Electron Microscope (FESEM). The electrical resistivity was determined using the four-point probe method controlled using a 12 K closed-cycle He-cryostat system working in the temperature range of 30 – 300

K. Four wires probe were attached on top and side of the rectangular bars using silver paint for the electrical contact. A Lake Shore 7130 AC magnetometer is used to measure the AC magnetic susceptibility as a function of temperature in 0.5 Oe magnetic fields at 295 Hz in the temperature range 70 - 120 K.

## RESULTS AND DISCUSSION

A quantitative analysis is often required to estimate the amount of Bi(Pb)-2212 and Bi(Pb)-2223 phases due to the coexistence of the Bi(Pb)-2212 phase in Bi(Pb)-2223 samples [6]. Figure 1 shows the XRD patterns of the sample doped with different $Eu_2O_3$ nanoparticles concentrations. All peaks were indexed with (•) for Bi(Pb)-2212 phases and (⁎) for Bi(Pb)-2223 phases. Eu-free sample showed peaks mostly belonged to Bi(Pb)-2223 phase and a few peaks belonging to the Bi(Pb)-2212 phase.

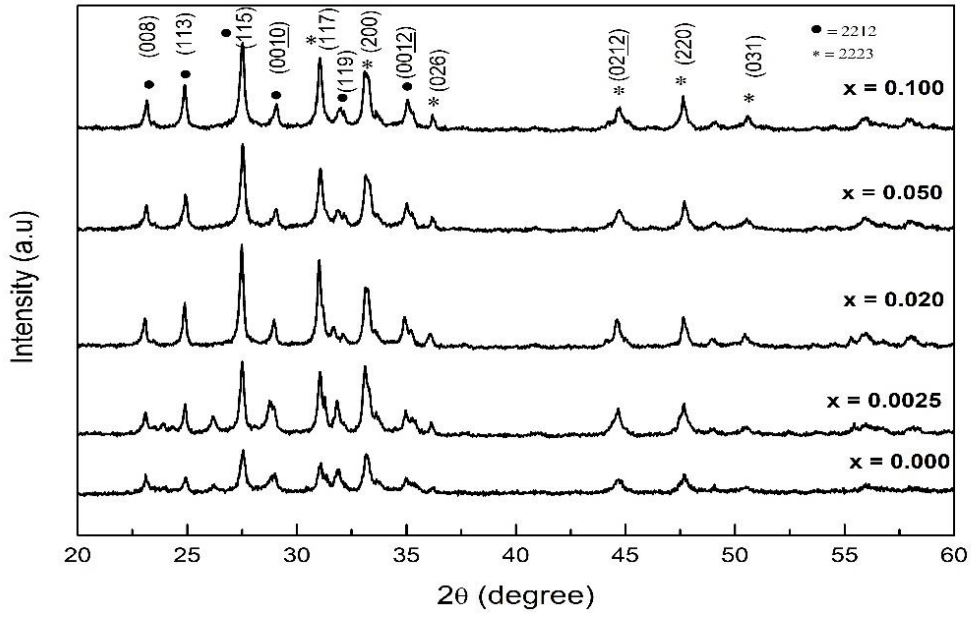


Figure 1: XRD patterns of Bi(Pb)-2223 doped $Eu_2O_3$ nanoparticles with different concentration

Observing the XRD patterns, the intensity of Bi(Pb)-2223 phase at peak (115) around $2\theta = 26.25°$ in $x = 0.0025$ sample increases than those of Eu-free sample. However, as Eu concentration $x > 0.0200$, the Bi(Pb)-2223 phase peak (115) finally vanished. Meanwhile, the Bi-2212 phase peak around $2\theta = 24.98°$ corresponded to (113) showed an increase in intensity because of increasing in the Eu substitution. The same observation with Bi(Pb)-2212 phase also can be seen around $2\theta = 27.54°$ corresponded to (115). Likewise, the characteristic in Bi(Pb)-2223 phase peaks (117) and (200) around $2\theta = 31.04°$ and $33.20°$ respectively also showed an increase in intensity compared to Eu-free sample. However, there is a slight decrement in intensity peaks for Bi(Pb)-2212 phase at $2\theta = 27.54°$ attributed to (119) because of increasing the Eu nanoparticles substitution.

The XRD peaks intensities that was observed can be used to calculate the relative volume fractions by using the following relations: [reference]

$$\mathrm{Bi(Pb)} - 2223 = \frac{\Sigma I(2223)}{\Sigma I(2223) + \Sigma I(2212)} \times 100\% \quad (1)$$

$$\mathrm{Bi(Pb)} - 2212 = \frac{\Sigma I(2212)}{\Sigma I(2223) + \Sigma I(2212)} \times 100\% \quad (2)$$

where *I*(2223) and *I*(2212) refer to the intensities of the Bi(Pb)-2223 and Bi(Pb)-2212 peaks, respectively. The calculated volume fractions of each phase are listed in Table 1.

Table 1 demonstrates the relative volume fraction of Bi(Pb)-2223 sample doped with different concentrations of Eu nanoparticles. As can be seen, increasing the amount of doping into the samples resulted in a decrease in the intensities of the peaks of 2223 phase. This result indicated that Pb substitution on Bi-site influences the kinetics of the formation of Bi(Pb)-2223 phases [7].

The corresponding lattice parameters were calculated from the least square method and (hkl) planes for tetragonal unit cell structure and tabulated in Table 1. As determined by the measured lattice parameter, the Eu-free sample has a tetragonal structure where a = b ≠ c. However, a slight change in crystal structure was observed from tetragonal to orthorhombic as Eu nanoparticle increased. Almost similar lattice parameter was observed by Hawa et al. [8] with the same stoichiometry. Increasing Eu nanoparticles concentration decreases the length of the c-axis, suggesting that Ca site has been substituted by a smaller size of Eu in all samples.

Table 1: Lattice parameter, relative volume fraction and crystallite size of BSCCO doped with different concentration of $Eu_2O_3$ nanoparticles

| Samples, *x* | Lattice parameter / Å | | | *V* / Å$^3$ | Volume fraction / % | | Crystallite size / nm |
|---|---|---|---|---|---|---|---|
| | *a* | *b* | *c* | | Bi-2223 | Bi-2212 | |
| 0.0000 | 5.399 | 5.399 | 37.095 | 1081.29 | 86.6 | 13.4 | 54.65 |
| 0.0025 | 5.406 | 5.402 | 37.178 | 1085.86 | 83.1 | 16.9 | 56.22 |
| 0.0200 | 5.392 | 5.421 | 37.070 | 1083.75 | 58.2 | 41.8 | 50.83 |
| 0.0500 | 5.386 | 5.398 | 36.790 | 1069.54 | 53.0 | 47.0 | 46.80 |
| 0.1000 | 5.385 | 5.393 | 36.493 | 1059.89 | 46.8 | 53.2 | 48.24 |

The crystallite size, $D$ of the sample was determined by applying Scherer equations [9]:

$$D = \frac{k\lambda}{B\cos\theta} \quad (3)$$

where $B$ is the FWHM of the X-ray peaks, $k$ is a shape factor without dimension with the value of 0.9, $\theta$ is the Bragg angle and $\lambda$ is the wavelength of X-ray (1.5406 Å). All the obtained $D$ values are recorded in Table 1. The crystallite size of the sample with $x$ = 0.0025 is slightly larger than that of Eu-free sample, indicating that $Eu_2O_3$ nanoparticles induced crystal growth in this sample by filling in the voids in the grain boundary network.

Figure 2 shows the graph of normalized resistivity versus temperature under zero magnetic field within a temperature range of 30-300 K for Bi(Pb)-2223 doped with different concentrations of $Eu_2O_3$ nanoparticles samples. The resistivity curve shows a smooth curvature which is Bi(Pb)-2223 phase single step for all prepared samples. As shown in Figure 2, sample with $x$ = 0.0025 Eu nanoparticles shows the highest resistivity with a $T_c$ of 94 K compared to Eu-free and other substituted samples. As Eu concentration increase up to $x$ = 0.0200, the resistivity values decrease to 52 K. The decrease in resistivity may be related to secondary phase formation as confirmed by XRD studies earlier.

As can be seen in Table 2, the transition width ($\Delta T_c = T_{c\ onset} - T_{c\ zero}$) was narrower for the sample with $x$ = 0.0200 concentration compared to the other samples. However, due to the lowest value of $T_{c\ onset}$ for this sample, these are not good results for the electrical resistance measurement. Meanwhile, the value of $\Delta T_c$ for sample with $x$ = 0.0025 is significantly lower than that of Eu-free sample indicating that inter-grain connectivity has been enhanced in substituted sample [10].

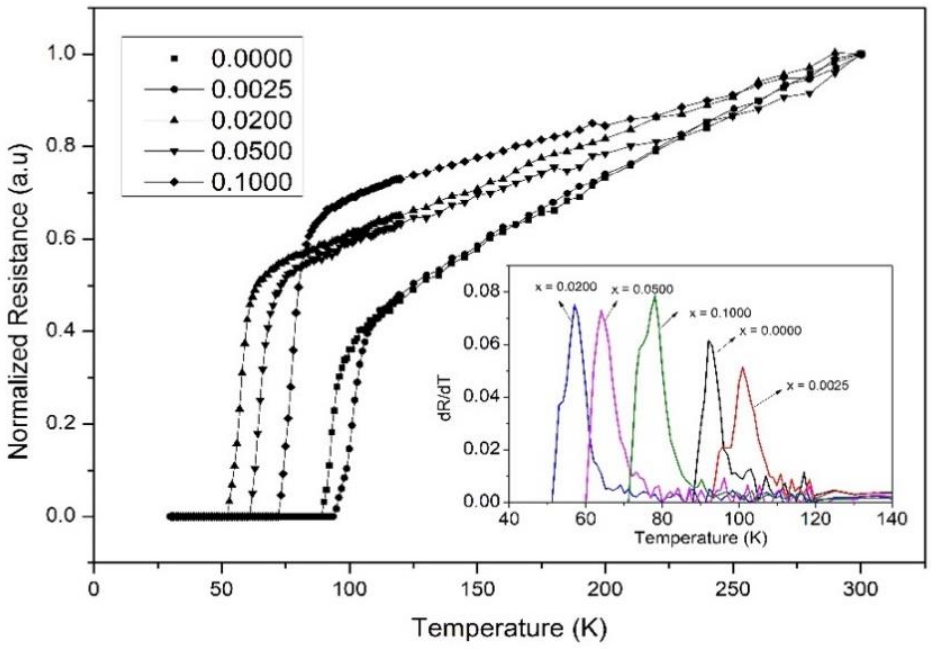


Figure 2: The normalized resistance versus temperature for Bi(Pb)-2223 doped with different concentration of $Eu_2O_3$ nanoparticles. Inset shows the *dR/dT* curve

corresponds to each concentration

Table 2: The critical temperatures $T_{c,onset}$, $T_{c,zero}$, $\Delta T_c$ and critical current density, $J_c$ of $Bi_{1.6}Pb_{0.4}Sr_2Ca_{2-x}Eu_xCu_3O_y$ ($x$ = 0.0000 – 0.1000) samples

| Samples, $x$ | Critical temperature / K | | | Critical current density, $J_c$ / A cm$^{-2}$ | | | | |
|---|---|---|---|---|---|---|---|---|
| | $T_{c\ onset}$ | $T_{c\ zero}$ | $\Delta T_c$ | 30 K | 40 K | 50 K | 60 K | 70 K |
| 0.0000 | 106 | 89 | 17 | 1.69 | 1.46 | 1.39 | 1.22 | 1.16 |
| 0.0025 | 108 | 94 | 14 | 2.77 | 2.59 | 2.31 | 1.94 | 1.57 |
| 0.0200 | 65 | 52 | 13 | 1.37 | 1.27 | 1.06 | - | - |
| 0.0500 | 76 | 61 | 15 | 1.57 | 1.35 | 1.24 | 1.01 | - |
| 0.1000 | 89 | 72 | 17 | 0.94 | 0.81 | 0.61 | 0.34 | - |

A four-point probe method was used to determine the critical current density, $J_c$ of all the samples, allowing the current to flow through the entire sample. Specials precautions were taken to ensure that the results were not influenced by heat at the active contacts. The critical current density, $J_c$ was calculated by using the following equation;

$$J_c = \frac{I_c}{A} \tag{4}$$

where $I_c$ is the critical current (A) and $A$ refers to the cross-sectional area of the sample (cm$^2$). As can be seen, Table 2 shows the critical current density, $J_c$ for samples with temperatures ranging from 30 K to 70 K measured in zero magnetic fields. The sample with $x$ = 0.0025 shows a maximum $J_c$ value which is much higher than Eu-free sample. It is possible that an improvement in intergrain connectivity might increase the effective area of the current flow, leading to an increase in $J_c$ values. It should be noted that a significant improvement of $J_c$ values can also be explained through enhancing conductivity between the grains therefore creating the new effective pinning centers. The $J_c$ values is found to decrease significantly for other Eu-doped samples. As the Eu concentration increases, the decrement in $J_c$ is likely caused by the increase of weak links between the superconducting grains, porosity, secondary phases, grain boundaries resistance and de-orienting of Bi(Pb)-2212 grains [11].

FESEM investigations were carried out on the fractured surface of the sample. Figure 3 displays FESEM images of Bi(Pb)-2223 doped with different concentration of $Eu_2O_3$ nanoparticles. As shown in Figure 3, FESEM micrographs presented a randomly distributed common flaky layers of plate-like grains. There was a clear grain boundary that was visible and connected to each other, which was in agreement with previous studies [12]. The micrograph image for $x$ = 0.0025 sample shows bigger and better grains alignment compared to the other substituted samples. This result is consistent with the calculated $J_c$ in the resistivity measurement where the improvement of grain boundary enhance the $J_c$ value of the sample. Nevertheless, increasing $Eu_2O_3$ nanoparticles concentration led to the degradation of grains hence form smaller plate-like structure that indicate phases of Bi(Pb)-2212 [8].

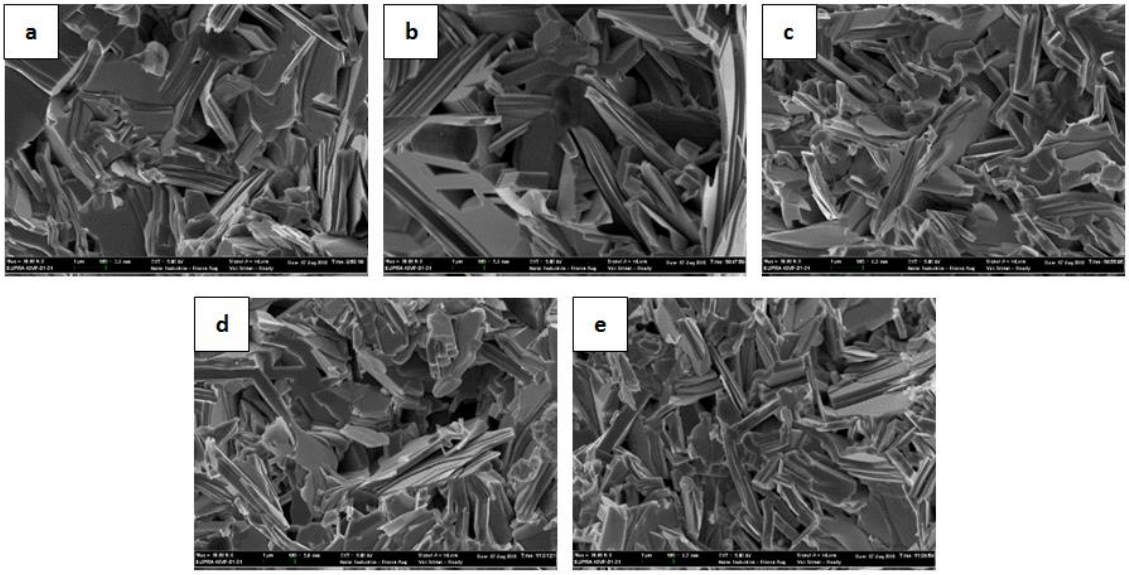


Figure 3: FESEM surface micrographs of Bi(Pb)-2223 doped with different concentration of $Eu_2O_3$ nanoparticles a) $x$ = 0.0000, b) $x$ = 0.0025, c) $x$ = 0.0200, d) $x$ = 0.0500, e) $x$ = 0.1000

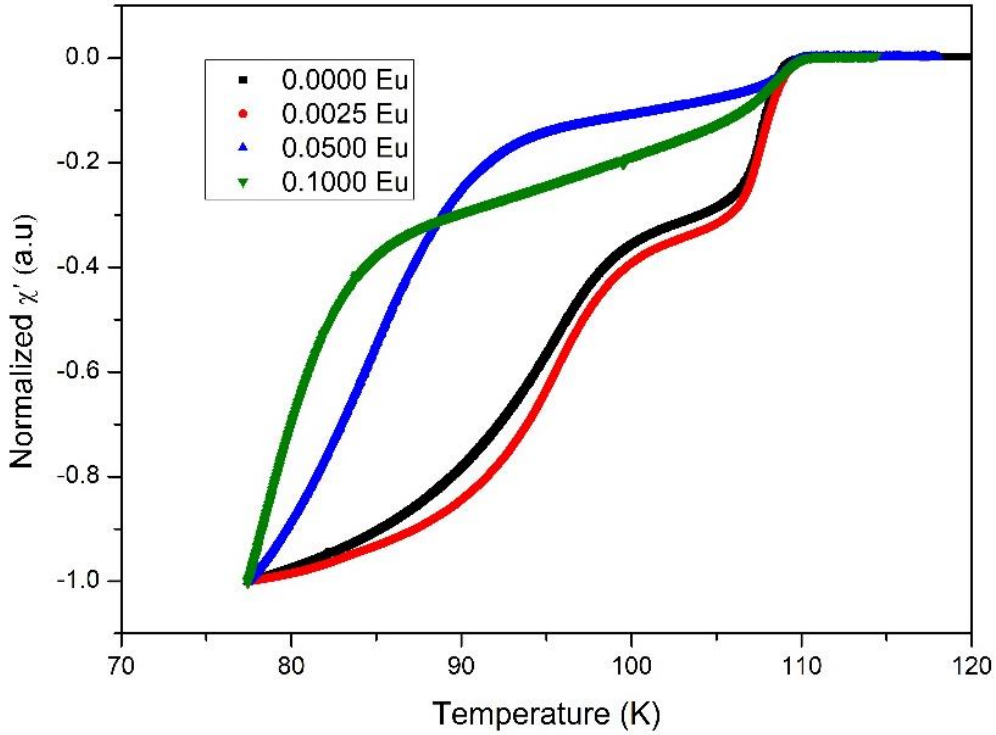


Figure 4: Real part of susceptibility versus temperature at different concentration of $Eu_2O_3$ nanoparticles for Bi(Pb)-2223

Figure 4 shows the temperature dependence of the real χ' part of susceptibility for all the

prepared samples. The magnetization measurements was done in the range of 77 K to 120 K at applied field of 0.5 Oe and frequency of 295 Hz. The real, χ' curves exhibited a two-step behavior for all sample. The diamagnetic transition in χ' occurs sharply in the first phase for Eu-free and $x$ = 0.0025 sample. It is figured that the point at which the susceptibility begins to fall, $T_{c\ onset}$ for pure sample is estimated to be 109 K in the real part, which is slightly higher (~3.0 K) than the one obtained from resistivity measurement. This increment might be related to the ACS measurement that use external magnetic field applied onto the whole bar sample compared to resistivity measurement that circulate only on the surface of sample. Meanwhile, a slower transition was seen in the second phase due to the weak links in the intergrain regions of the samples. Hence, it can be stated that the second phase in χ' part referred to the intergrain coupling transition [13].

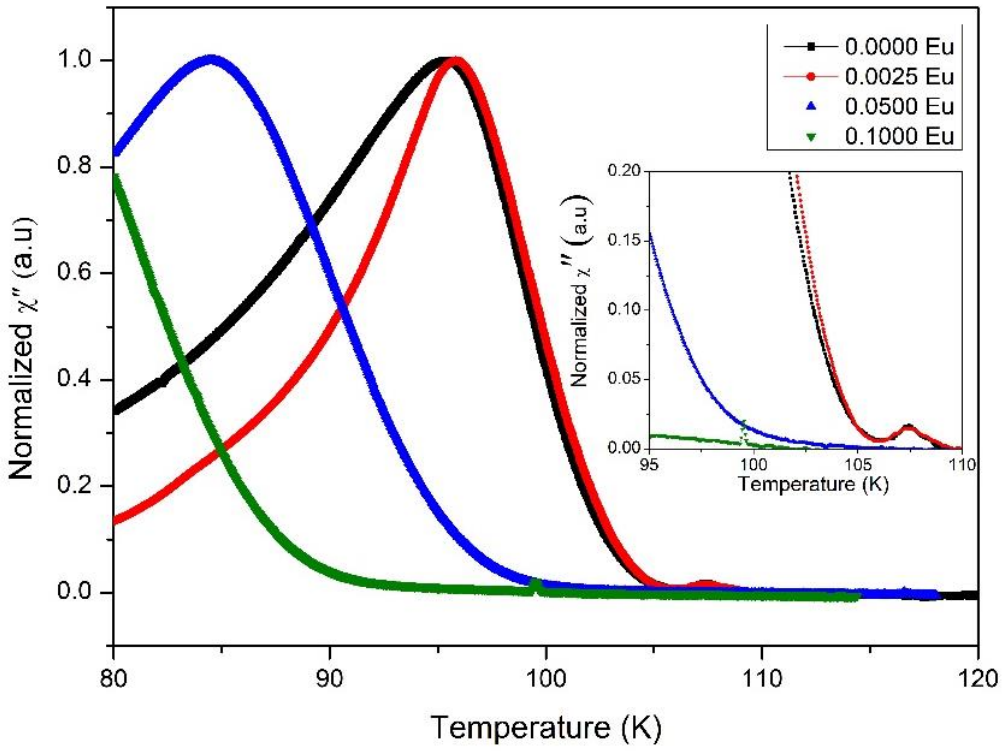


Figure 5: Imaginary part of susceptibility versus temperature at different concentration of $Eu_2O_3$ nanoparticles for Bi(Pb)-2223. Inset shows the evolution of intragranular peaks, $T_{pm}$ for each sample

As shown in Figure 5, the imaginary χ'' part are useful in analyzing the nature of weak links in high temperature superconductor. From Figure 5, it can be seen that the peaks of χ'' shifts to lower temperature as Eu concentration increased. The highest value for intergranular peaks, $T_{pj}$ is seen for the sample $x$ = 0.0025 at 95 K. This behavior might be due to the strong link between the grains which leads to the increase in critical current density, $J_c$ [14]. At the same time, intragranular peak, $T_{pm}$ were observed at 107 K, 108 K and 99 K for sample with $x$ = 0.0000, 0.0025 and 0.1000 respectively.

## CONCLUSION

In this research, the structural and superconducting properties of Bi(Pb)-2223 samples doped with different concentration of Eu nanoparticles produced through solid state method were analyzed. It was found that the volume fraction of Bi(Pb)-2223 phase decreased as the Eu concentration increased. The results of the resistivity measurement show that the highest value of $T_{c\ zero}$ and $J_c$ for the doped sample corresponded at $x$ = 0.0025 sample. As the concentration of Eu nanoparticles increased, the crystallite size calculated from the XRD peaks intensities decreased. The surface morphology was observed via FESEM micrographs which show that Eu nanoparticles doping favors the formation of flaky layers of plate-like grains with random distribution. Also, the ac susceptibility results reveal that as Eu concentration increases, the peaks of $\chi''$ shifts to lower temperatures. Hence, the present study indicate that $x$ = 0.0025 is the best concentration in Bi(Pb)-2223 superconductor as it enhances the superconducting parameters ($T_c$ and $J_c$) compared to the Eu-free sample.

## ACKNOWLEDGEMENTS

The authors wish to thank Ministry of Higher Education Malaysia (MOHE) for financial support to carry out this research through Fundamental Research Grant Scheme (FRGS) no. 600-RMI/FRGS 5/3 (74/2016).

## REFERENCES

[1] Fallah-Arani, H., Baghshahi, S., Sedghi ,A., Stornaiuolo, D., Tafuri, F., Massarotti, D. and Riahi-Noori, N. *Ceram. Int.* **44** (5) 5209–5218 (2018)
[2] Abbas, M. M., Abass, L. K. and Salman, U. *Energy Procedia* **18** 215–224 (2012)
[3] Zelati, A., Amirabadizadeh, A., Kompany, A., Salamati, H. and Sonier, J. *J. Supercond. Nov. Magn.* **27**(6) 1369–1379 (2014)
[4] Shalaby, M. S., Hashem, H. M., Hammad, T. R., Wahab, L. A., Marzouk, K. H. and Soltan, S. *J. Radiat. Res. Appl. Sci.* **9**(3) 345–351 (2016)
[5] Mohamed, S. B., Halim, S. A. and Azhan, H. *IEEE Trans. Appl. Supercond.* **11**(1) 2862–2864 (2001)
[6] Albiss, B. A., Obaidat, I. M., Gharaibeh, M., Ghamlouche, H. and Obeidat, S. M. *Solid State Commun.* **150**(33-34) 1542–1547 (2010)
[7] Anis-Ur-Rehman, M. and Mubeen, M. *Synth. Met.* **162**(19–20) 1769–1774 (2012)
[8] Hawa, J. S., Azhan, H., Yahya, S. Y., Azman, K., Hidayah, H. N. and Norazidah, A. W. *J. Supercond. Nov. Magn.* **26**(4) 979–983 (2013)
[9] He, K., Chen, N., Wang, C., Wei, L. and Chen, J. *Cryst. Res. Technol.* **53**(2) 1–6 (2018)
[10] Kocabaş, K. and Çiftçioğlu, M. *Phys. Status Solidi Appl. Res.* **177**(2) 539–545 (2000)
[11] Bal, S., Dogruer, M., Yildirim, G., Varilci, A., Terzioglu, C. and Zalaoglu, Y. *J. Supercond. Nov. Magn.* **25**(4) 847–856 (2012)

[12] Hamadneh, I., Agil, A., Yahya, A. K. and Halim, S. A. *Phys. C Supercond. its Appl.* **463–465** 207–210 (2007)
[13] Ghahfarokhi, S. E. M. and Joola, F. *Chin. J. Phys.* **54** 921–930 (2016)
[14] Saoudel, A., Saoudel, A., Boudjadja, Y., Bouchekhou, H., Allag, H. and Altintas, S. P. *Cryogenics* **117** 103326 (2021)